Supplementary Information

Nickel iron phosphide ultrathin nanosheets anchored on nitrogen-doped carbon nanoflake arrays as bifunctional catalyst for efficient overall water splitting

Jialin Bian[1+], Zeyi Song[1+], Xianglin Li[2, 3], Yuzhong Zhang[1*], Chuanwei Cheng[1, 2*]

[1]Shanghai Key Laboratory of Special Artificial Microstructure Materials and Technology, School of Physics Science and Engineering, Tongji University, Shanghai 200092, P. R. China.

[2]Hunan First Normal University, Changsha, Hunan, 410205, P. R. China.

[3]Dongguan NanoFrontier Microelectronics Equipment Co., Ltd, Dongguan, Guangdong, 523808 P. R. China

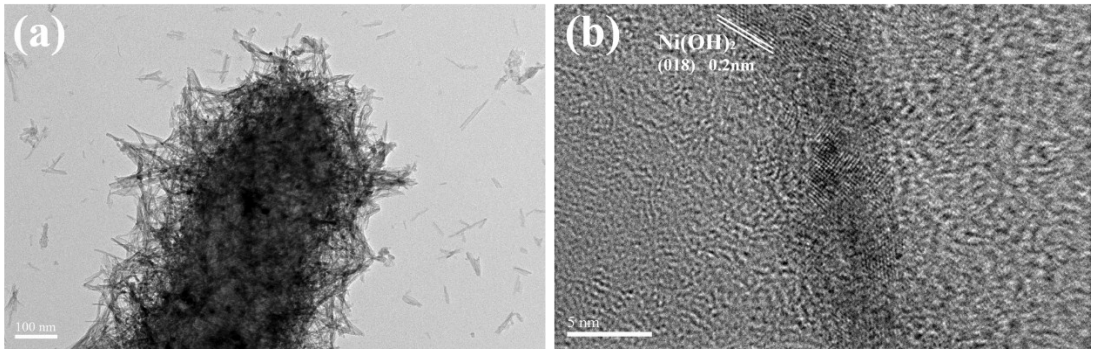

Figure S1. (a) TEM image and (b) HR-resolution image of the CC-NC-NiFe LDH.

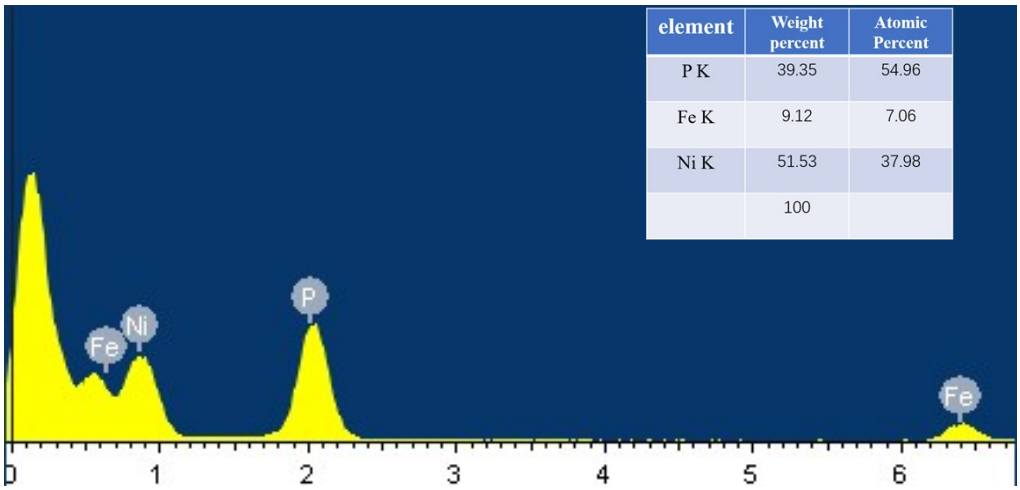

Figure S2. The EDX spectra f CC-NC-NiFeP

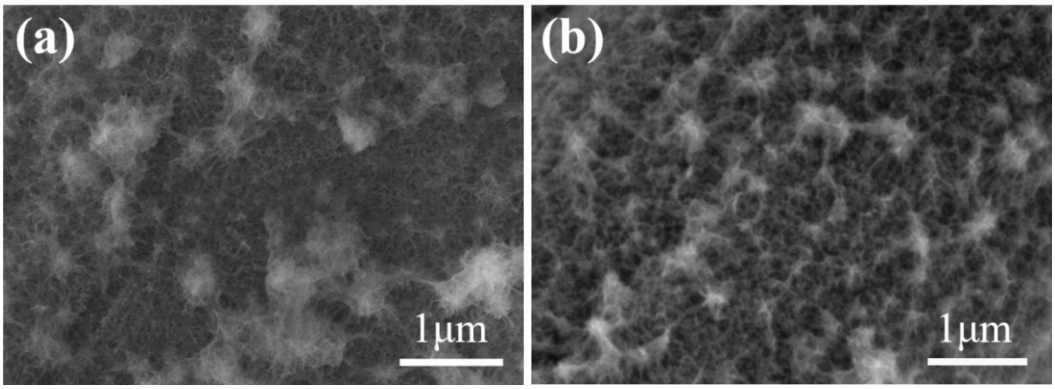

Figure S3. (a) SEM image of the CC-NiFe LDH. (b) SEM images of the CC-NiFeP

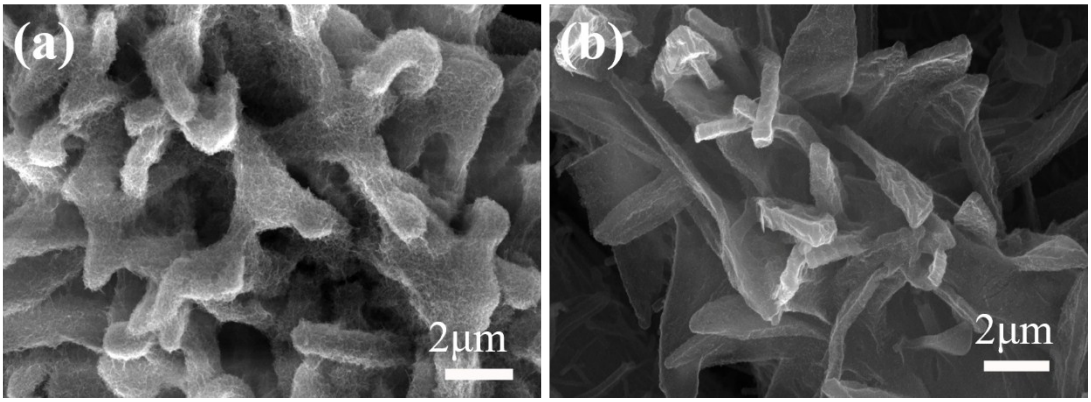

Figure S4. (a) SEM image of the CC-NC-Ni_2P. (b) SEM images of the CC-NC-Fe_2P

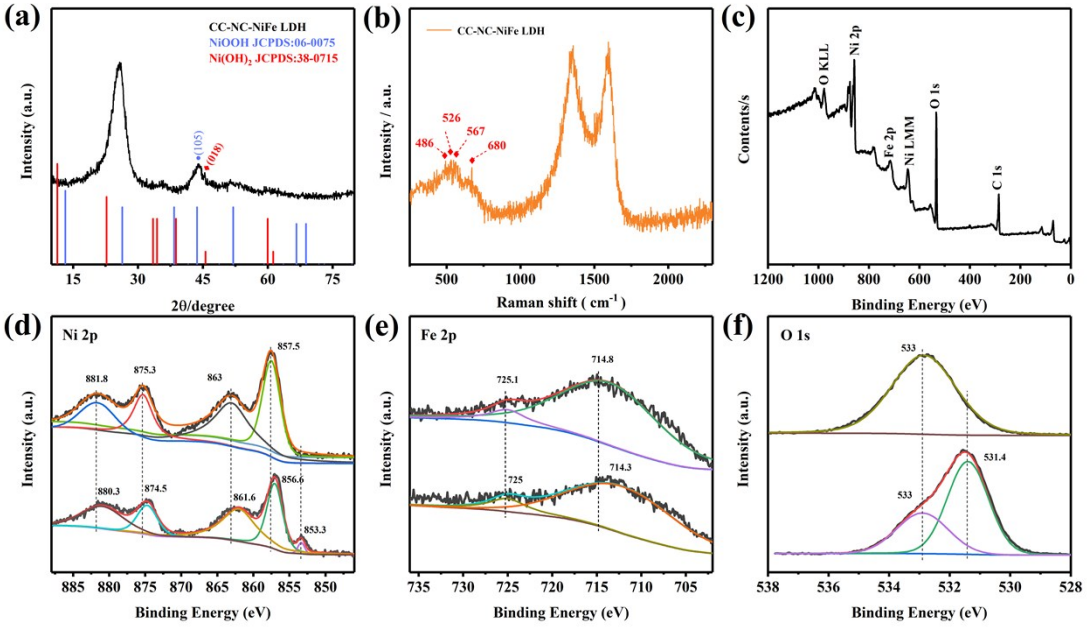

Figure S5. (a) XRD of CC-NC-NiFe LDH (b) Raman spectra of CC-NC-NiFe LDH. (c) overall XPS spectra of CC-NC-NiFe LDH (d-f) high-resolution scans of Ni 2p, Fe 2p and N 1s spectra of CC-NC-NiFe LDH and CC-NC-NiFeP

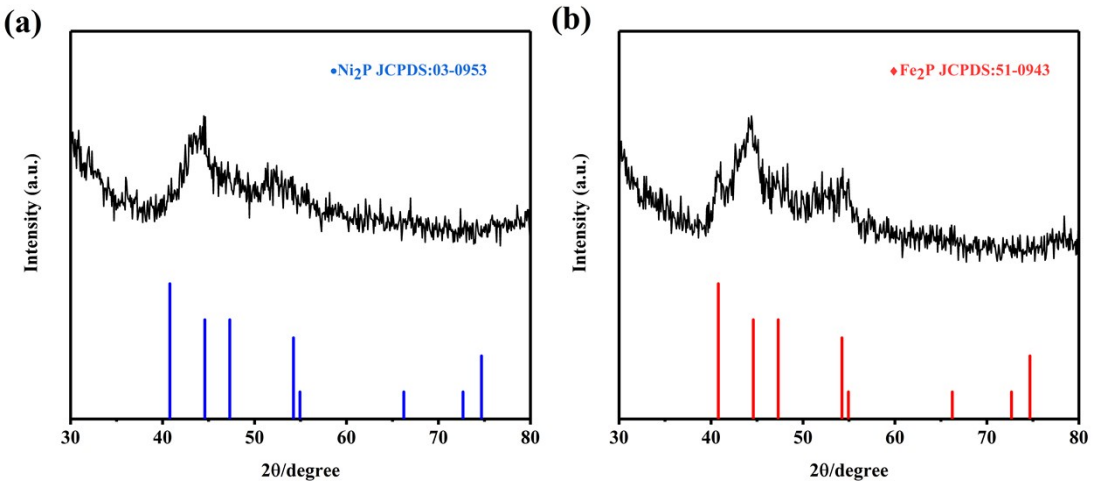

Figure S6. (a-b)XRD of CC-NC-Ni_2P and CC-NC-Fe_2P

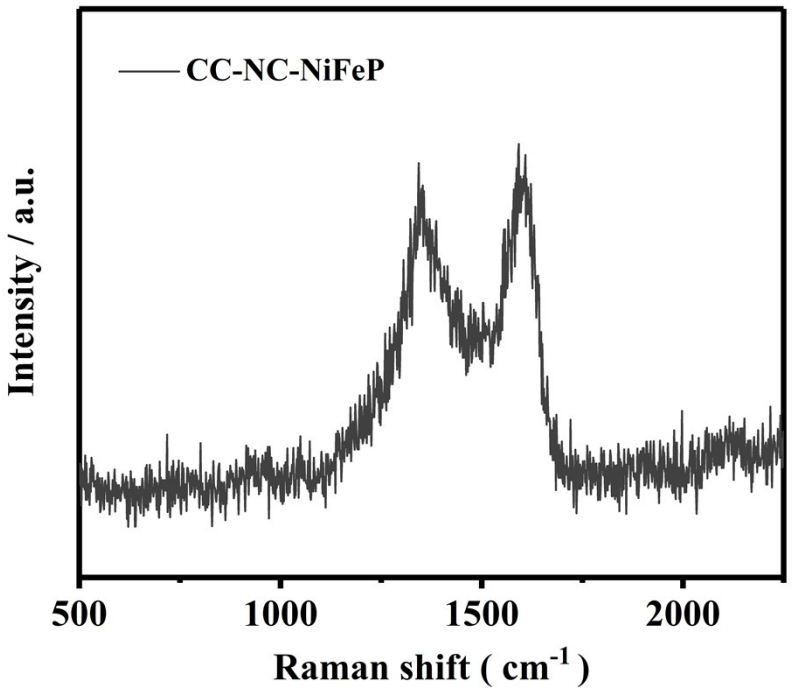

Figure S7. Raman spectrum of CC-NC-NiFeP.

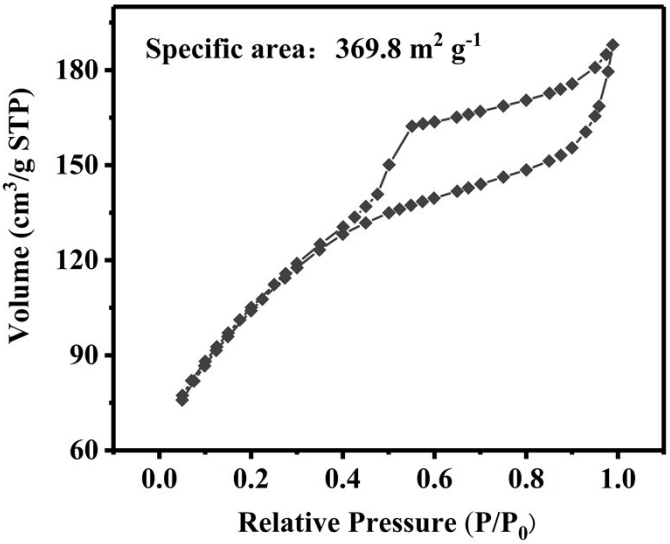

Figure S8. N_2 adsorption and desorption isotherms of MOF-derived carbon nanoflakes powders.

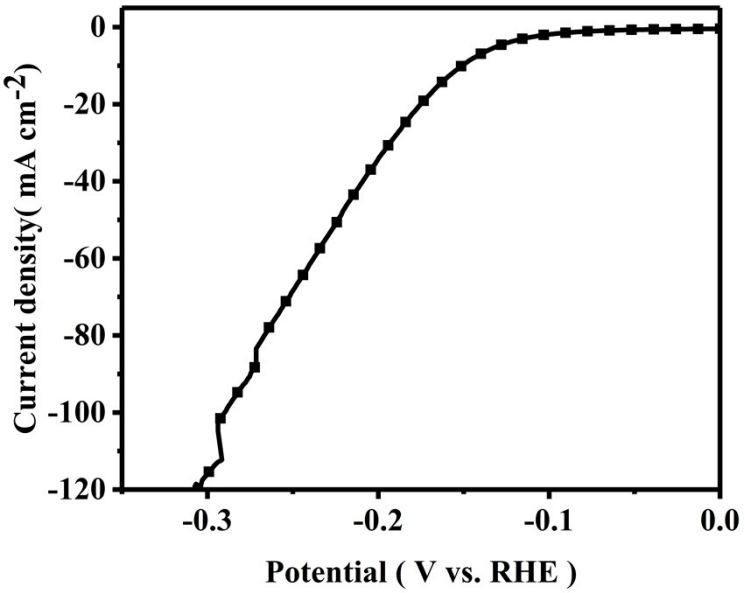

Figure S9. HER polarization curves of CC-NC-NiFeP in 0.5 M H_2SO_4.

Table S1 A compaprison of the HER performance of CC-NC-NiFeP in 1M KOH with non-precious metal catalyst in recent reports

Catalyst	**η (mV) at J = 10 mA cm^{-2}**	**Tafel solpe (mV dec^{-1})**	**Loading (mg cm-2)**	**Reference**
CC-NC-NiFeP	**94**	**70**	**2.67**	**This work**
Ni/$Mo_2C_{(1:2)}$-NCNFs	143	57.8	1.4	R1
$Ni_3ZnC_{0.7}$/NCNT-70	203	91	0.8	R2
$NiCo_2S_4$ & $NiCo_2S_4$	183	89.8	1.5	R3
$NiCo_2S_4$/NF	80	58.5	-	R4
NiFeP/SG	125	47	2.07	R12
$Co_{0.6}Fe_{0.4}P$-1.125	133	61	-	R7
Ni_3S_2@MoS_2/FeOO	95	88	-	R8
Fe-Co-P/NF	163	106.1	-	R9
NiFe LDH@NiCoP/	120	88.2	-	R11

\

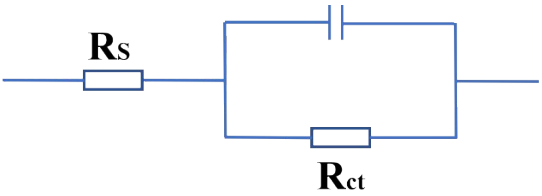

Figure S10. equivalent circuit diagram

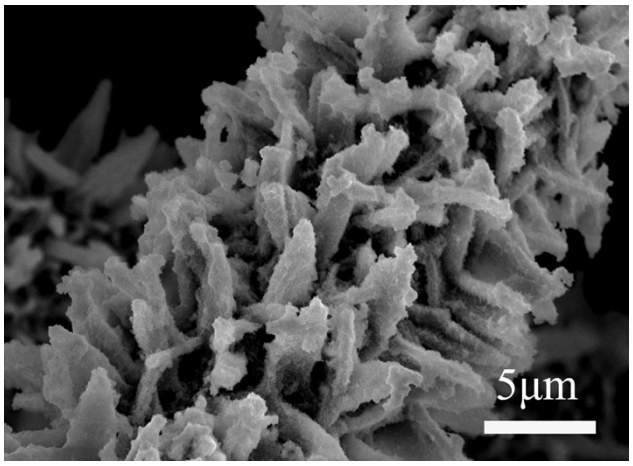

Figure S11. SEM image of CC-NC-NiFeP after HER stability test.

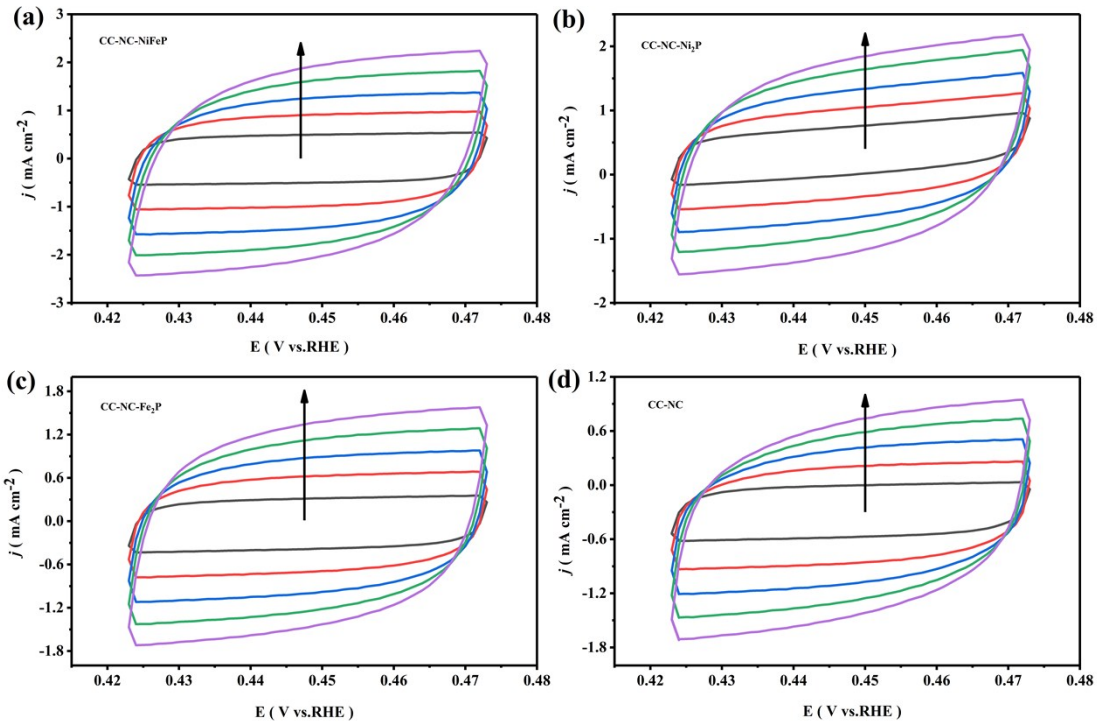

Figure S12. CV curves for (a) CC-NC-NiFeP, (b) CC-NC-Ni_2P and (c) CC-NC-Fe_2P and (d)CC-NC.

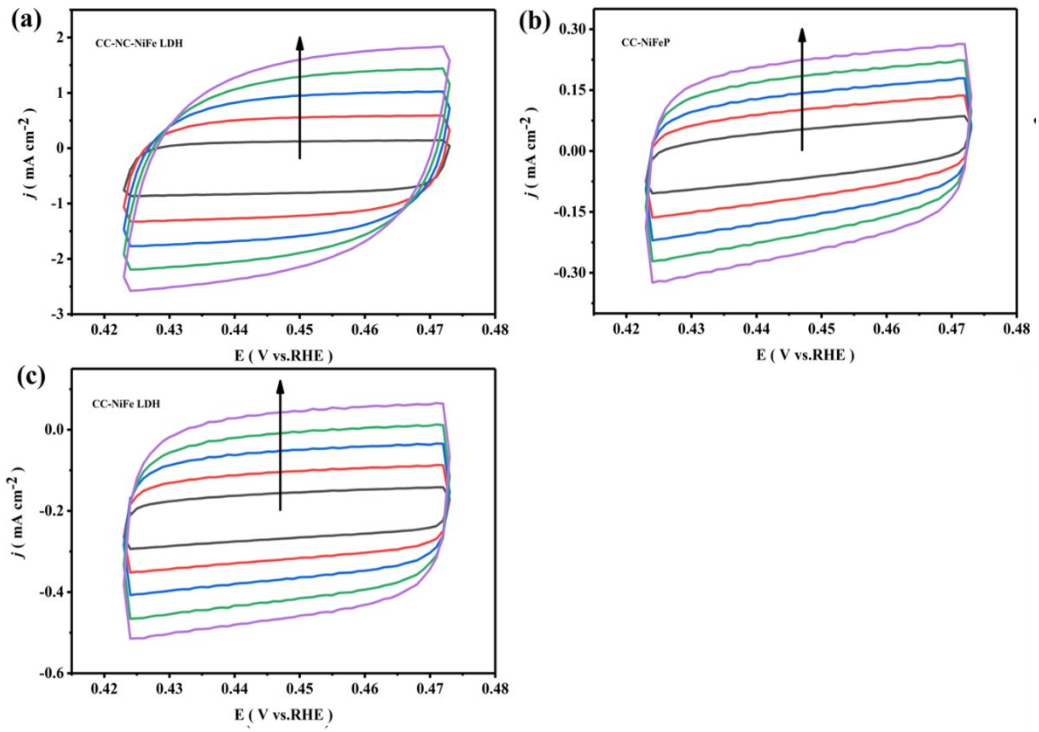

Figure S13. (a-c) CV curves for CC-NC-NiFe LDH, CC-NiFeP and CC-NiFe LDH.

Table S2 A compaprison of the OER performance of CC-NC-NiFeP in 1M KOH with non-precious metal catalyst in recent reports

Catalyst	η (mV) at J = 10 mA cm^{-2}	Tafel solpe (mV dec^{-1})	Loading (mg cm-2)	Reference
CC-NC-NiFeP	**145** J_{100}**=270**	**67**	**2.67**	**This work**
Ni/$Mo_2C_{(1:2)}$-NCNFs	288	78.4	0.8	R1
$Ni_3ZnC_{0.7}$/NCNT-700	380	89	1.5	R2
$NiCo_2S_4$ & $NiCo_2S_4$	280	86.8	-	R3
$NiCo_2S_4$	243	54.9	2.07	R4
CoP-Co_2P@PC/PG	J_{20}=272	66	-	R5
Ni–Fe–P/NF30	229	-	-	R6
$Co_{0.6}Fe_{0.4}$P-1.125	298	48	-	R7
Ni_3S_2@MoS_2/FeOOH	234	49	-	R8
Fe-Co-P/NF	250	49.2	-	R9
Ni_2P-Ni_3S_2 HNAs/NF	210	62	-	R10
NiFe LDH@NiCoP/Nl	220	48.6	-	R11
NiFeP/GC	218	44	-	R12

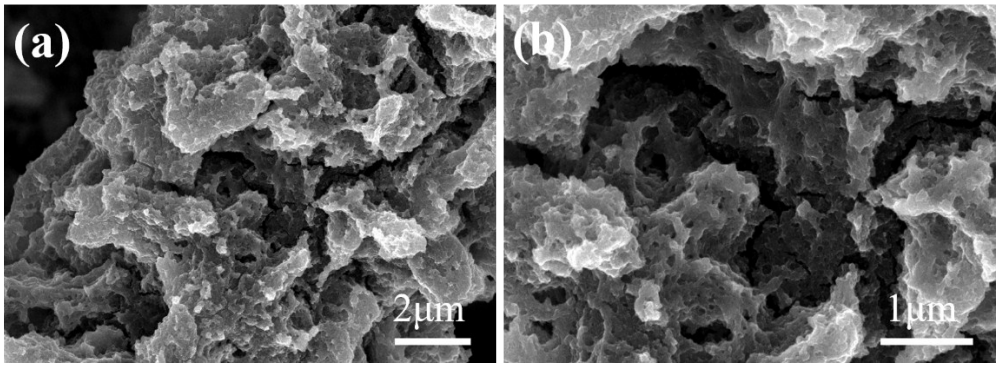

Figure S14. SEM images of CC-NC-NiFeP after the OER stability test

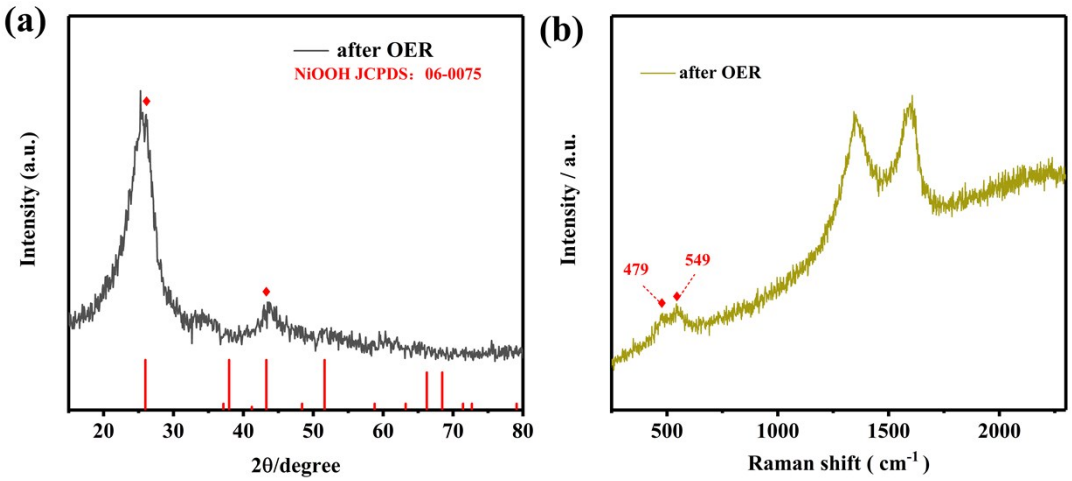

Figure S15. (a) XRD and (b) Raman spectrum of CC-NC-NiFeP after OER stability test.

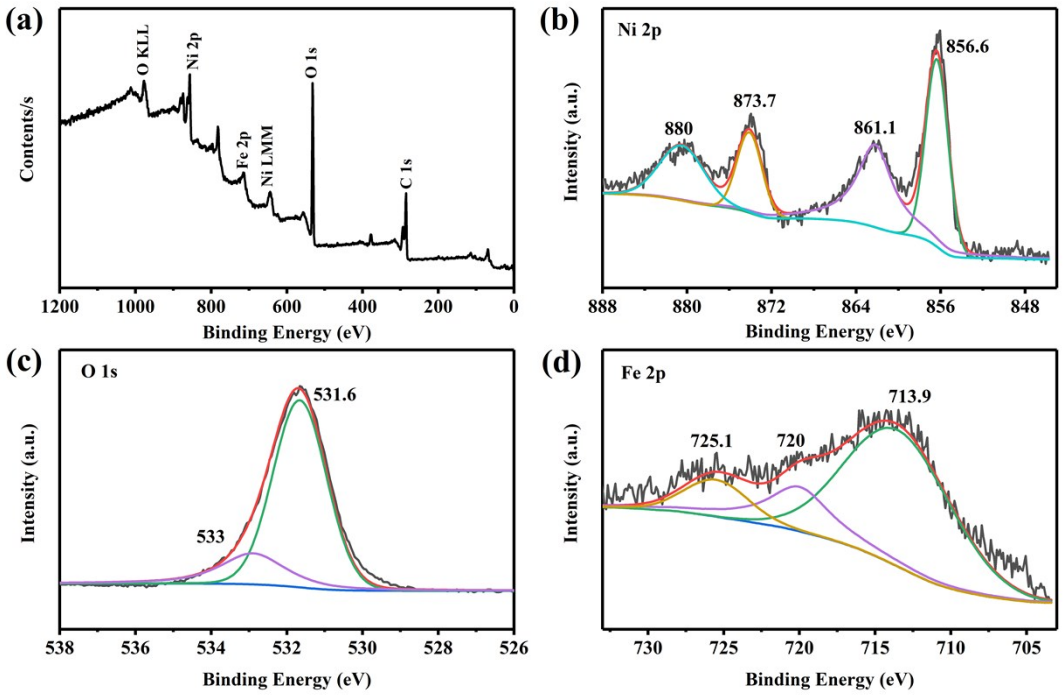

Figure S16. (a) Overall XPS spectra of CC-NC-NiFeP after the OER stability test (b-d) High-resolution scans of nickel, iron, and oxygen of CC-NC-NiFeP after OER stability test

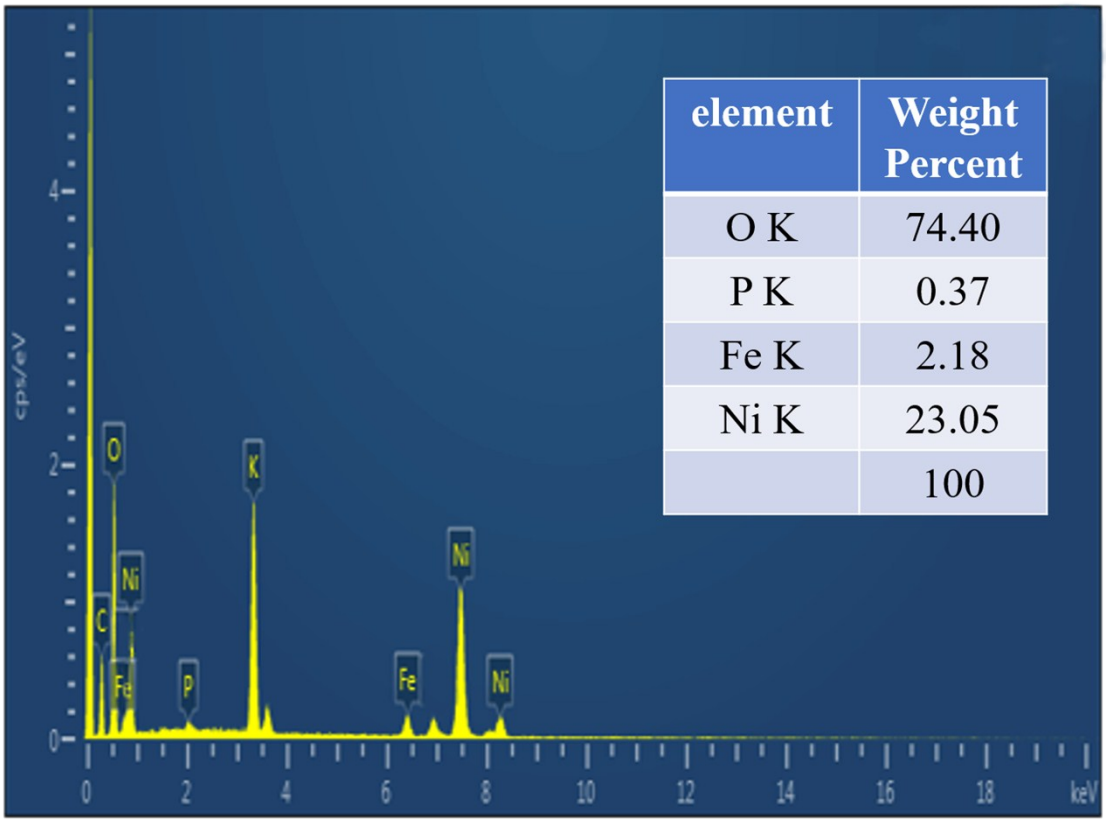

element	Weight Percent
O K	74.40
P K	0.37
Fe K	2.18
Ni K	23.05
	100

Figure S17. The EDX spectra of CC-NC-NiFeP after the OER stability test.

Computational detail

Theoretical models

Ni_2P (201), Fe_2P (201) and surface oxidized Ni_2P (201) (denoted as Ni_2P-O) were modeled by a periodically repeated four-layer slab and a vacuum region of 20 Å was used to separate adjacent slabs. An unit cell in the plane perpendicular to (201) direction were used for Ni_2P (201), Fe_2P (201) and Ni_2P-O as shown in Figure 6 a. For the case of Fe doping for Ni_2P, totally four Ni atoms are replaced by Fe atoms where one of these substituted Ni atoms are on the surface, the other are in the slab, as displayed in Figure 6 a and Figure S10 b. The crystal structures of these catalysts for both hydrogen evolution reaction and oxygen evolution reactions were optimized. The lattice constants of the slab for Ni_2P (201), Fe-doped Ni_2P (201) and their counterparts with partial surface oxidation are 8.95 Å, 5.8751 Å, and 27.5191 Å, and that of Fe_2P (201) are 8.959 Å, 5.6568 Å, and 27.4129 Å. In all structural relaxation calculations, the bottom two layers of slabs were fixed and the top two layers with adsorbed atoms were allowed to relax.

Free energy calculation

The free energy of atomic hydrogen adsorption is a widely accepted descriptor of hydrogen evolution reaction activity, which is read

$\Delta G_H^* = \Delta E(H^*)+\Delta ZPE(H^*)-T\Delta S(H^*)$

with the hydrogen chemisorption energy

$$\Delta E(H^*) = E_{slab+H}-(E_{slab}+\frac{1}{2}E_{H2})$$

Where E_{slab+H} refers to the total energy of slab with a hydrogen atom absorbed on the surface, E_{slab} refers to the total energy of slab with clean surface, E_{H2} refers to the energy of H_2 in the gas phase. $\Delta ZPE(H^*)$ denotes the change of zero point energy of hydrogen between the absorbed state and the gas phase. $\Delta S(H^*)$ represents the entropy change of H^* adsorption. Since the configuration entropy in the adsorbed state is small and negligible, we take the entropy of adsorption of $\frac{1}{2}H_2$ as $\Delta S(H^*) \approx -\frac{1}{2}S(H_2)$, where $S(H_2)$ is the entropy of H_2 in the gap phase at stand conditions. Hence the free energy of atomic hydrogen adsorption can be approximately obtained through $\Delta G_H^* \approx \Delta E(H^*)+\Delta ZPE(H^*)+0.205$ eV, due to $TS(H_2) \approx 0.41$ eV for H_2 at stand conditions.

The overall OER process can be described by the following four electron reaction paths:

$H_2O(l)+* \rightleftarrows HO* + H^+ + e^-$ (1)

$HO* \rightleftarrows O* + H^+ + e^-$ (2)

$O^*+H_2O(l) \rightleftarrows HOO^*+ H^+ +e^-$ (3)

$HOO^* \rightleftarrows * + O_2(g) +H^+ +e^-$ (4)

By using the scheme described in the previous study[13], the Gibbs free energy of each elementary step for OER has been calculated as shown in the main text.

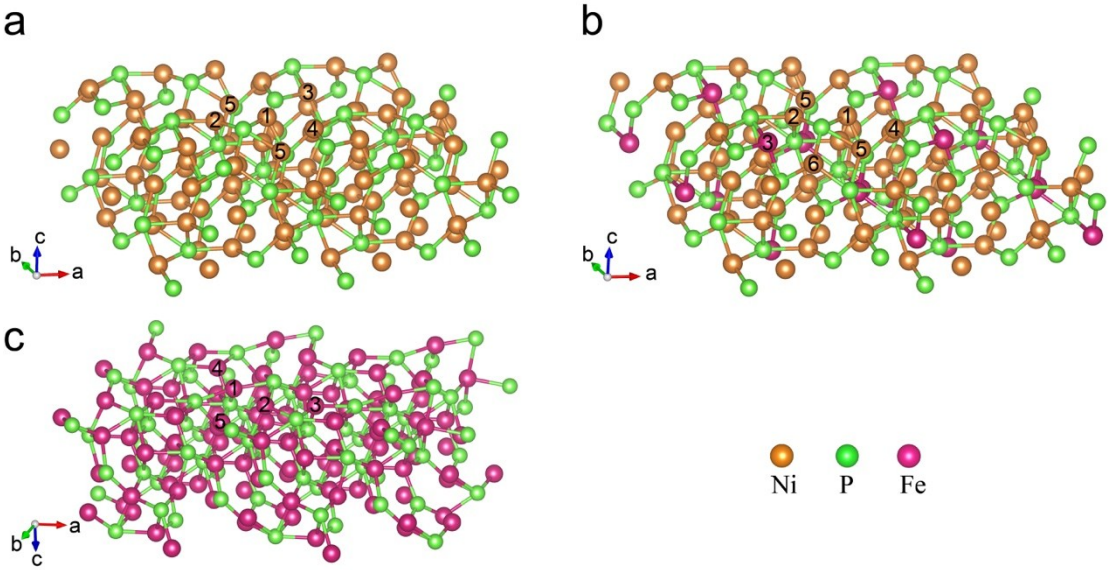

Figure S18 theoretical models used in the work. The crystal structure of (a) Ni_2P (201), (b) $Ni_{1.7}Fe_{0.3}P$ (201), and (c) Fe_2P (201). The Ni atoms and Fe atoms on the surfaces of these catalysts are labeled by integers.

Table S3. The calculated results of H^* absorbed on the surface of Ni_2P, $Ni_{1.7}Fe_{0.3}P$, and Fe_2P in different models. $\Delta E(H^*)$ denotes the hydrogen chemisorption energy, $ZPE(H^*)$ the zero point energy, ΔZPE the zero point change, and $\Delta G(H^*)$ the adsorption free energy. While 'm-H-n' denotes the bridge active sites between two atoms labeled by 'm' and 'n', 'Hollow' represents the hollow active sites on the top of the center of the triangular formed by nearest-neighbor Ni or Fe atoms labeled 1, 2, and 5 on the surface. The corresponding theoretical models are shown in Fig. S18.

models	adsorption site	$\Delta E(H^*)$/eV	$ZPE(H^*)$/eV	ΔZPE/eV	$\Delta G(H^*)$/eV
Ni_2P	1-H-4	-0.391	0.190	0.052	-0.134
Ni_2P	Hollow	-0.219	0.171	0.034	0.020
Ni_2P	3	0.100	0.186	0.048	0.354
Fe_2P	1-H-4	-0.809	0.184	0.047	-0.558
Fe_2P	Hollow	-0.737	0.187	0.050	-0.482
Fe_2P	3	-0.071	0.177	0.040	0.174
$Ni_{1.6}Fe_{0.4}P$	1-H-4	-0.426	0.190	0.053	-0.169
$Ni_{1.6}Fe_{0.4}P$	3-H-6	-0.256	0.183	0.046	-0.006
$Ni_{1.6}Fe_{0.4}P$	Hollow	-0.435	0.161	0.024	-0.206

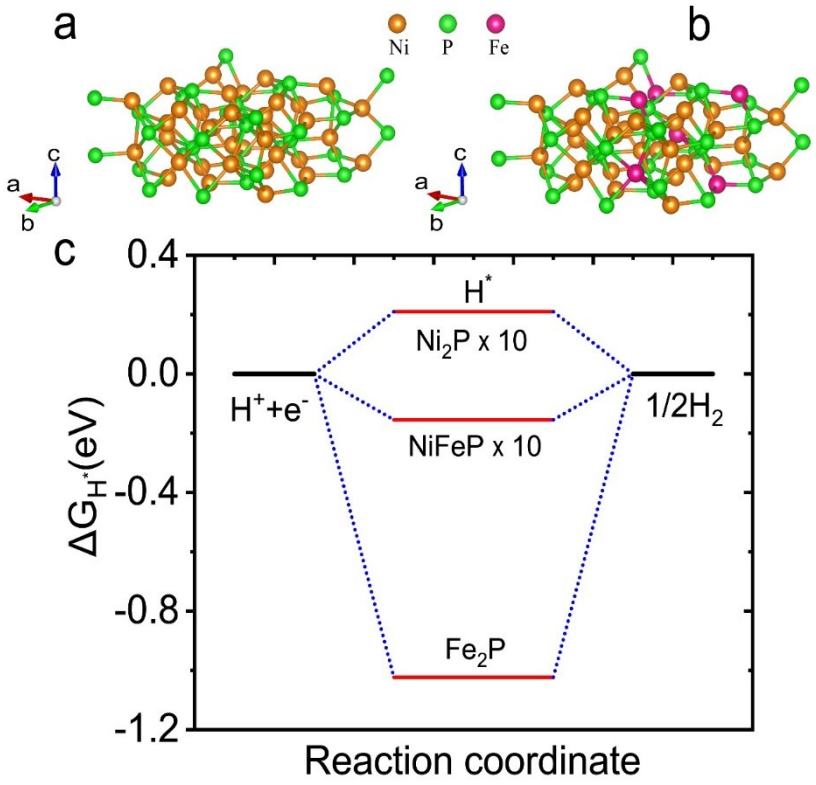

Figure S19**.** Theoretical models and the free-energy diagram of hydrogen evolution reaction. Crystal structure of (a) Ni_2P (001) and (b) $Ni_{1.7}Fe_{0.3}P$ (001); (c) Free-energy diagram of hydrogen evolution reaction over Ni_2P (001), $Ni_{1.7}Fe_{0.3}P$ (001) and Fe_2P (001).

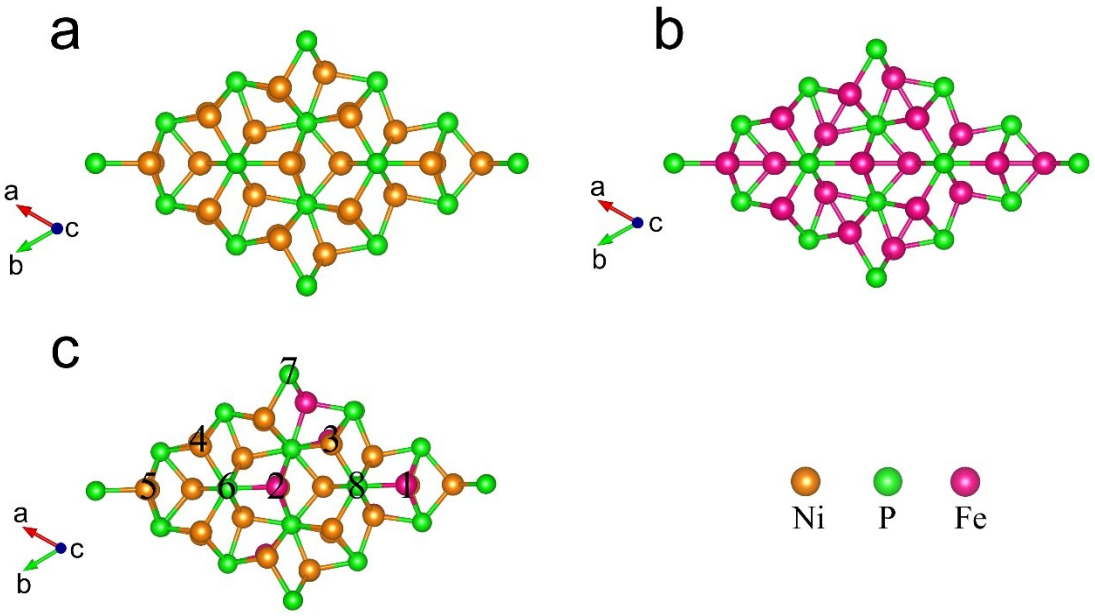

Figure S20 theoretical models used in the work. (a) Ni_2P (001), (b) Fe_2P (001), and (c) the crystal structures of $Ni_{1.7}Fe_{0.3}P$ (001) for which the partial Ni atoms on the surface are labeled 3, 4, and 5, and the Fe atoms on the surface are labeled 1 and 2, and the partial P atoms on the surface are labeled 6, 7, and 8.

Table S4. The calculated results of H^* absorbed on the surface of Fe_2P, $Ni_{1.7}Fe_{0.3}P$, and Ni_2P in different models. $\Delta E(H^*)$ denotes the hydrogen chemisorption energy, $ZPE(H^*)$ the zero point energy, ΔZPE the zero point change, and $\Delta G(H^*)$ the adsorption free energy. While 'm-H-n' denotes the bridge active sites between two atoms labeled by 'm' and 'n', 'Hollow' represents the hollow active sites on the top of the center of the triangular formed by nearest-neighbor Ni atoms on the surface. The corresponding theoretical models are shown in Fig. S20.

models	adsorption site	$\Delta E(H^*)$/eV	$ZPE(H^*)$/eV	ΔZPE/eV	$\Delta G(H^*)$/eV
Fe_2P	Hollow	-1.261	0.170	0.032	-1.023
Ni_2P	Hollow	-0.192	0.145	0.008	0.021
$Ni_{1.7}Fe_{0.3}P$	4-H-5	-0.252	0.169	0.032	-0.015
$Ni_{1.7}Fe_{0.3}P$	3	-0.514	0.174	0.036	-0.273
$Ni_{1.7}Fe_{0.3}P$	4	-0.505	0.171	0.033	-0.267
$Ni_{1.7}Fe_{0.3}P$	6	0.207	0.180	0.042	0.454
$Ni_{1.7}Fe_{0.3}P$	7	0.076	0.189	0.052	0.333
$Ni_{1.7}Fe_{0.3}P$	8	0.272	0.176	0.039	0.516

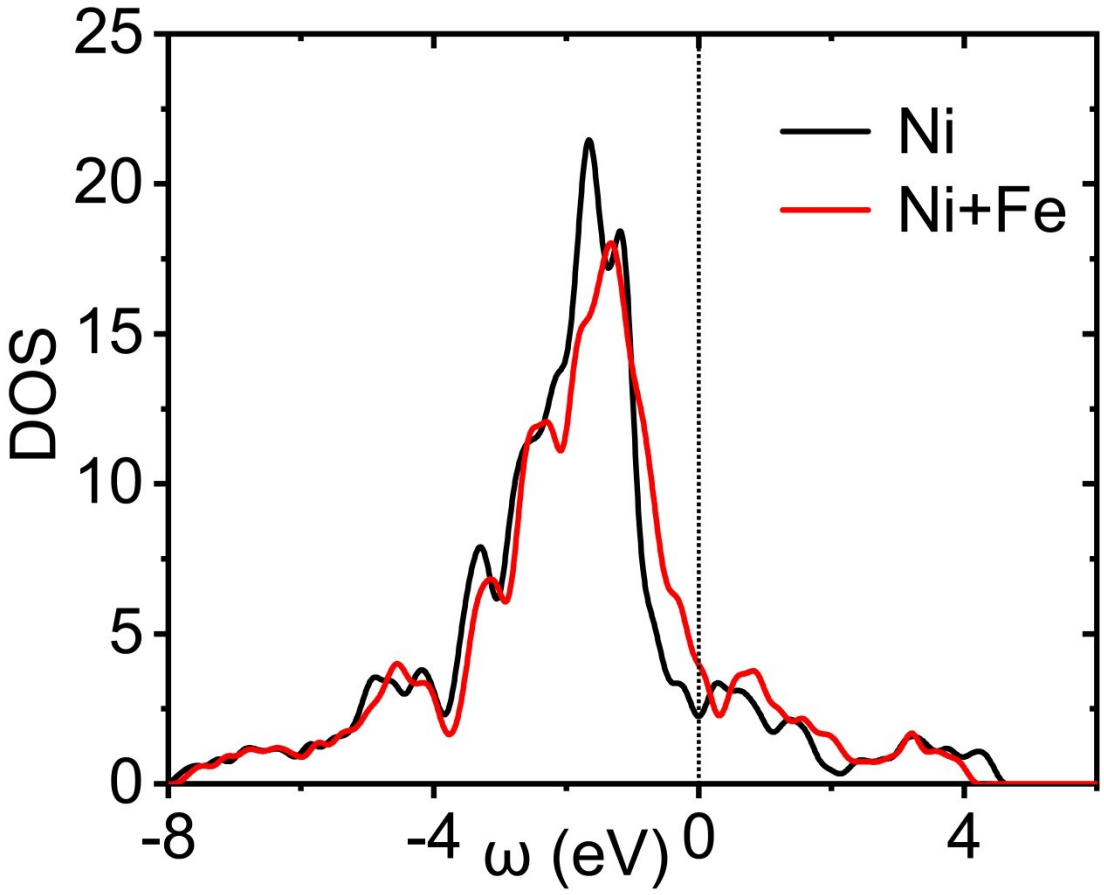

Figure S21 Total and projected density of states of Ni_2P and Fe-doped Ni_2P.

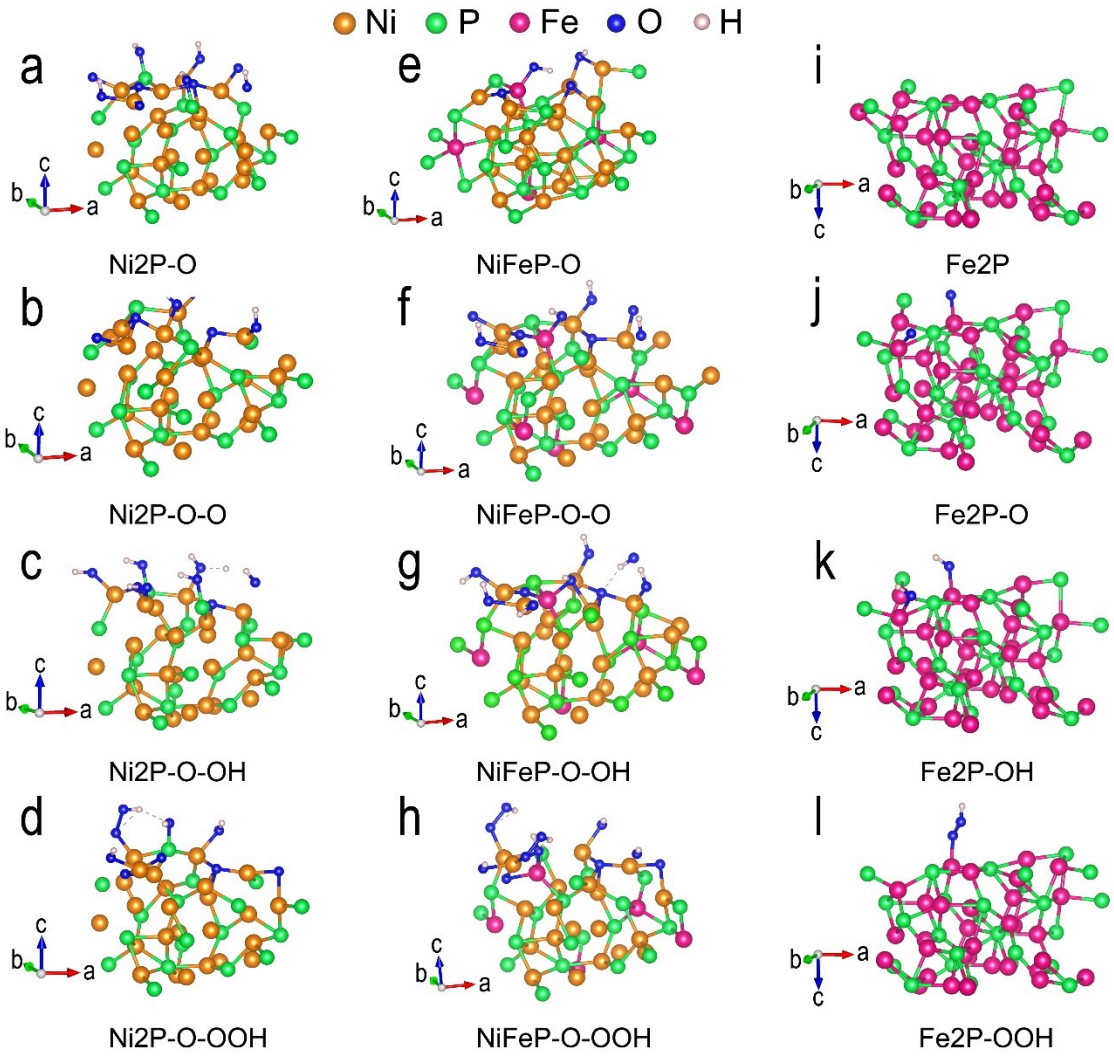

Figure S22 View of adsorption of intermediates on catalyst surfaces in four elemental steps during OER. (a-d) Ni_2P (201) with partial surface oxidation, (e-h) $Ni_{1.7}Fe_{0.3}P$ (201) with partial surface oxidation, and (i-l) Fe_2P (201).

References

1. M. Li, Y. Zhu, H. Wang, C. Wang, N. Pinna, and X. Lu, *Adv. Energy. Mater.*, 2019, **9** , 1803185.
2. R. Li, X. Li, D. Yu, L. Li, G. Yang, K. Zhang, S. Ramakrishna, L. Xie, and S. Peng, *Carbon*, 2019, **148**, 496
3. F. Li, R. Xu, Y. Li, F. Liang, D. Zhang, W.-F. Fu, and X.-J. Lv, *Carbon*, 2019, **145**, 521.
4. Z. Kang, H. Guo, J. Wu, X. Sun, Z. Zhang, Q. Liao, S. Zhang, H. Si, P. Wu, L. Wang, and Y. Zhang, *Adv. Funct. Mater.*, 2019, **29**,1807031.
5. J. Yang, D. Guo, S. Zhao, Y. Lin, R. Yang, D. Xu, N. Shi, X. Zhang, L. Lu, Y. Q. Lan, J. Bao, and M. Han, *Small*, 2019, **15**, 1804546.
6. K. Wang, K. Sun, T. Yu, X. Liu, G. Wang, L. Jiang, and G. Xie, *J. Mater. Chem. A*, 2019, **7**, 2518.
7. Y. Lian, H. Sun, X. Wang, P. Qi, Q. Mu, Y. Chen, J. Ye, X. Zhao, Z. Deng, and Y. Peng, *Chem. Sci*, 2019, **10**, 464.
8. M. Zheng, K. Guo, W.-J. Jiang, T. Tang, X. Wang, P. Zhou, J. Du, Y. Zhao, C. Xu,
   and J.-S. Hu, *Appl. Catal. B: Environ.*, 2019, **244**, 1004.
9. K. Sun, K. Wang, T. Yu, X. Liu, G. Wang, L. Jiang, Y. Bu, and G. Xie, *Int. J. Hydrogen Energy*, 2019, **44**, 1328.
10. L.Y. Zeng, K. Sun, X.B. Wang, Y.Q. Liu, Y. Pan, Z. Liu, D.W. Cao, Y. Song, S.H. Liu, C.G. Liu, *Nano Energy* ,2018,**51**,26.
11. H. Zhang, X. Li, A. Hähnel, V. Naumann, C. Lin, S. Azimi, S. L. Schweizer, A. W. Maijenburg, and R. B. Wehrspohn, *Adv. Func. Mater.*, 2018, **28**, 1706847 .
12. R.-Q. Li, B.-L. Wang, T. Gao, R. Zhang, C. Xu, X. Jiang, J. Zeng, Y. Bando, P. Hu, Y. Li, and X.-B. Wang, *Nano Energy*, 2019, **58**, 870.
13. I. C. Man, H. Y. Su, F. Calle-Vallejo, H. A. Hansen, J. I. Martínez, N. G. Inoglu, J. Kitchin, T. F. Jaramillo, J. K. Nørskov, and J. Rossmeisl, *ChemCatChem*, 2011, **3**, 1159.